A Pandas complex adapted for piRNA-guided transposon silencing

Kang Zhao[#1], Sha Cheng[#2], Na Miao[#1], Ping Xu[#1,3], Xiaohua Lu[#1], Ming Wang[1], Yuhan Zhang[2], Xun Yuan[2], Weiwei Liu[1], Xin Lu[1], Xuan Ouyang[1], Peng Zhou[1], Jiaqi Gu[1,4], Yiqun Zhang[1], Ding Qiu[1], Shan Wang[1], Zhaohui Jin[2], Youzhong Wan[3], Jinbiao Ma[4], Ying Huang[2,5], Yang Yu[1,5]

[1]Institute of Biophysics, Key Laboratory of RNA Biology, Chinese Academy of Sciences, University of Chinese Academy of Sciences, Beijing, China, 100101
[2]State Key Laboratory of Molecular Biology, Shanghai Key Laboratory of Molecular Andrology, CAS Center for Excellence in Molecular Cell Science, Shanghai Institute of Biochemistry and Cell Biology, Chinese Academy of Sciences, University of Chinese Academy of Sciences, Shanghai, China, 200031
[3]School of Life Sciences, National Engineering Laboratory of AIDS Vaccine, Key Laboratory for Molecular Enzymology and Engineering of Ministry of Education, Jilin University, Changchun, Jilin, China, 130012
[4]State Key Laboratory of Genetic Engineering, Department of Biochemistry, School of Life Sciences, Fudan University, Shanghai, China, 200438

[#]contributed equally

[5]correspondence: yuyang@ibp.ac.cn; huangy@sibcb.ac.cn

Keywords: piRNA, transposon silencing, dNxf2, Panoramix, crystal structure, *Drosophila*, dNxf1/TAP, dNxt1/p15

Abstract

The repression of transposons by the Piwi-interacting RNA (piRNA) pathway is essential to protect animal germ cells. In *Drosophila* ovaries, Panoramix (Panx) enforces transcriptional silencing by binding to the target-engaged Piwi-piRNA complex, although the precise mechanisms by which this occur remain elusive. Here, we show that Panx functions together with a germline specific paralogue of a nuclear export factor, dNxf2, and its cofactor dNxt1 (p15) as a ternary complex to suppress transposon expression. Structural and functional analysis demonstrate that dNxf2 plays critical roles in Panx association via its UBA domain, and transposon silencing through binding to transposon transcripts directly. Furthermore, dNxf2 interacts with dNxf1 (TAP), which, unexpectedly, is also required for Panx-mediated silencing. Therefore, we propose that dNxf2 may function as a Pandas (Panoramix-dNxf2 dependent TAP/p15 silencing) complex, which counteracts the canonical RNA exporting machinery (TAP/p15) and restricts transposons to nuclear peripheries.

53 To maintain eukaryotic genome integrity, nascent transcripts of transposons are often targeted by
54 nuclear Argonaute proteins for transcriptional gene silencing (TGS)(*1-5*). In animal gonads, the
55 PIWI-clade Argonautes guided by piRNAs (PIWI-interacting RNA) are thought to recognize nascent
56 transposon transcripts and direct sequence-specific heterochromatin formation(*3*). As a critical
57 cofactor of *Drosophila* nuclear Piwi, Panoramix (Panx, also known as Silencio) links the target-
58 engaged Piwi-piRNA complex to the general silencing machinery(*6*, *7*). Enforced tethering of Panx
59 to nascent transcripts leads to cotranscriptional silencing and correlates with deposition of histone
60 H3 lysine 9 trimethylation (H3K9me3) marks(*6*, *7*). However, the mechanism by which Panx
61 mediates the repression remains unknown.
62
63 We cross-examined proteins that co-immunoprecipitated with Panx (fig. S1A) with piRNA
64 pathway candidate genes from RNA interference (RNAi) screens(*8-11*). Unexpectedly, we
65 identified dNxf2 as a potential cofactor of Panx (fig. S1A-C). dNxf2 belongs to an evolutionarily
66 conserved NXF (nuclear export factor) family of proteins, yet depletion of dNxf2 had no effect on
67 polyadenylated mRNA export(*12*, *13*). Instead, dNxf2 and its cofactor dNxt1 (also known as p15)
68 were both identified in two published RNAi screens as being essential for transposon silencing(*8*,
69 *9*). Similar to Panx, dNxf2 is specifically expressed in female gonads (fig. S1D).
70
71 To validate the interaction between Panx and dNxf2, we performed GFP immunoprecipitation
72 from ovaries expressing GFP-Panx fusion under its native promoter. Results of mass spectrometry
73 analysis (fig. S1B) and western blotting demonstrated that endogenous dNxf2 is associated with
74 Panx (Fig. 1A). Likewise, Halo-tagged dNxf2 was able to precipitate endogenous Panx proteins
75 from Ovarian Somatic Cell (OSC) lysates (Fig. 1B). We next tested if dNxf2 is functionally required
76 for Panx-mediated silencing. The luciferase transcripts with BoxB sites in their 3′ untranslated
77 regions are repressed if λN-Panx is tethered(*6*, *7*). The luciferase expression was then measured

upon germline-specific knockdowns of dNxf2 or dNxt1 (Fig. 1C). Despite λN-Panx tethering, loss of either dNxf2 or dNxt1 significantly weakened the ability of Panx to repress the reporter, as compared to the controls (Zuc or attp2, Fig. 1C). Consistent with the reporter de-repression, transposon transcripts are elevated upon dNxf2 RNAi (fig. S1E). Taken together, our data suggests that dNxf2 and dNxt1 may function as a heterodimer either with or downstream of Panx to suppress transposon expression.

Next, we used RNA sequencing (RNA-seq) to examine global effects on transposon expression with germline-specific knockdowns of dNxf2, compared with Panx RNAi (Fig. 1D-F). As expected, dNxf2 knockdown triggered a dramatic increase of transposon transcripts (Fig. 1D). The effect is similar to that of Panx (Fig. 1E-F), suggesting that dNxf2 is specifically required for silencing of transposons repressed by Panx. To rule out off-target effects of RNAi, we generated mutants of dNxf2 using CRISPR/Cas9 (fig. S2A)(*14*). Although the mutation we isolated removed just 20 amino acids from the N-terminus of dNxf2, mutant female flies were sterile (fig. S2B), similar to other core piRNA pathway mutants(*6*). Loss of dNxf2 had essentially no effect on Piwi nuclear localization or stability (fig. S2C-D), consistent with dNxf2's function as an effector protein. Furthermore, dNxf2 mutants showed global up-regulation of transposons (fig. S2E-G) and de-repression of the luciferase reporter despite λN-Panx tethering (fig. S3A). We noticed here that the endogenous Panx protein level is significantly reduced in the absence of dNxf2 (fig. S2D). To rule out the possibility that dNxf2 might affect transposons indirectly via Panx stability, we measured transposon expression upon overexpressing λN-Flag-Panx under the dNxf2 mutant background (fig. S3A-E). Consistently, dNxf2 mutant female flies lost transposon control (fig. S3C-D) and were complete sterile despite the overexpression of λN-Flag-Panx (fig. S3E).

The striking phenotypic similarities between dNxf2 and Panx prompted us to test whether these

103 two proteins interact directly. Therefore, we used yeast two-hybrid (Y2H) assays to determine the
104 interacting regions. The domain architecture of dNxf2 is very similar to that of the canonical RNA
105 export factor, dNxf1/TAP (also known as sbr, Fig. 2A). Both proteins contain leucine-rich repeats
106 (LRR), an RNA recognition motif (RRM), a nuclear transport factor 2 (NTF2)-like domain, and a
107 ubiquitin-associated domain (UBA). Interestingly, Panx only interacts with the UBA domain of dNxf2
108 (Fig. 2B). This interaction is specific as the UBA domain of dNxf1 showed no binding (Fig. 2B).
109 Surprisingly, however, neither full length nor the NTF2-UBA fragment of dNxf2 could bind Panx
110 (Fig. 2B), suggesting that the UBA domain of dNxf2 might be in a "closed" conformation in the
111 presence of the NTF2 domain. Additionally, the interactions between dNxt1 and the NTF2 domains
112 of either dNxf2 or dNxf1 are significantly weakened in the presence of its UBA domain (Fig. 2C).
113 Since *Drosophila* Nxt1 is absent in yeast, we tested whether dNxt1 might release the UBA domain
114 from the NTF2 domain to permit Panx binding. Indeed, ectopic expression of dNxt1 is sufficient to
115 allow full length dNxf2 to interact with Panx in a yeast-three hybrid assay (Fig. 2D). Next, we
116 mapped the minimum region of Panx down to residues 315-343 (NIR, dNxf2 interacting region) as
117 sufficient for UBA binding (Fig. 2E and fig. S3I). Consistent with the fact that dNxt1 forms a
118 heterodimer with dNxf2(*12*), we found that dNxt1 co-migrates with a fusion protein comprised of
119 $dNxf2^{NTF2\text{-}UBA}$-$(Gly\text{-}Ser)_4$-$Panx^{NIR}$ by size-exclusive chromatography (Fig. 2F), suggesting that Panx,
120 dNxf2, and dNxt1 may exist as a ternary complex. Indeed, purified $Panx^{NIR}$ forms a stable complex
121 with the UBA domain of dNxf2 with a dissociation constant of ~3.2 μM (Fig. 2G). Despite many
122 efforts, we failed to crystalize the $dNxf2^{NTF2}$ domain. Therefore, we determined the crystal structure
123 of $dNxf1^{NTF2}$ in complex with dNxt1 and modelled the binding of $dNxf2^{NTF2}$ to dNxt1 (fig. S4A).
124 Consistent with the Y2H results, $dNxf2^{NTF2}$ maintained most, if not all, residues that interact with
125 dNxt1 (fig. S4A-E).
126
127 To further explore the molecular basis of interactions between dNxf2 and Panx, we determined

128 the structure of the dNxf2-Panx complex (Fig. 3A-D). The structure was solved to a 1.5-Å resolution
129 (Table S1). dNxf2^{UBA} forms a compact three-helix bundle (α1–α3) with a 3_{10}-helix (η1) at the C-
130 terminus (Fig. 3B). The Panx^{NIR} is folded into a long α-helix and lays on the hydrophobic surface
131 formed by α2 and α3 (Fig. 3B-C and fig. S4F). A324, A328, V331, L332, and I335 on Panx interact
132 with V800, F819, F826, F840, L823 and I827 on dNxf2 via hydrophobic interactions (Fig. 3D).
133 Moreover, R321 and R327 on Panx form salt bridges with D837 and E799 on Nxf2^{UBA}, respectively
134 (Fig. 3D). To validate the intermolecular interactions between dNxf2 and Panx, we mutated key
135 residues of the interacting interface (Fig. 3E). While either L823A or D837A single point mutation
136 affected the binding between Panx and dNxf2^{UBA}, the double point mutation of dNxf2^{UBA}
137 F826A/I827A nearly abolished the interactions with Panx in both Y2H and co-immunoprecipitation
138 assays (Fig. 3E-F), highlighting the significant contribution of these residues in Panx binding.
139
140 Having demonstrated direct binding between dNxf2 and Panx, we next tested the functional
141 importance of this interaction. We took advantage of a previously described λN/BoxB luciferase
142 reporter system to see if artificial tethering of dNxf2 could lead to repression. Indeed, we observed
143 significant repression upon tethering of a λN-dNxf2 fusion protein (Fig. 3G), unlike that of the
144 negative controls (λN-YFP or GFP-dNxf2 lacking a λN-tag). Similar to Panx, the level of λN-dNxf2
145 mediated repression appeared to be dosage-dependent, as it correlated with the number of BoxB
146 binding sites (Fig. 3H). Most importantly, the repression is dependent on the presence of the dNxf2
147 UBA domain (Fig. 3G, dNxf2-ΔUBA).
148
149 Our structure provided insight into why dNxf2^{UBA} prefers to bind the silencing factor Panx rather
150 than the FG repeats of the nuclear pore complex (NPC). In contrast to the highly charged surface
151 of the Nxf1-type UBA (i.e. hsNxf1 or scMex67), dNxf2^{UBA} favors hydrophobic binding with Panx
152 (Fig. 3C and fig. S5A-B). Key residues on the interacting interface are highly conserved among

153 different *Drosophila* species but altered in the Nxf1-type UBA (fig. S5A). On the opposite surface
154 of the Nxf1-type UBA, a hydrophobic pocket is formed to accommodate the FxFG peptide of the
155 NPC (fig. S5C-D). However, this pocket is missing in dNxf2^{UBA} due to a salt bridge formed between
156 K829 and E814 (fig. S5C). Additionally, the bulky side chain of L825 on dNxf2^{UBA} may hinder FG
157 binding (fig. S5C). In contrast, the corresponding amino acids in hsNxf1 (A602) or scMex67 (G583)
158 contain much smaller side chains (fig. S5C-D), therefore, give space for FxFG interactions.
159 Consistent with the structural prediction, dNxf2^{UBA} failed to interact with the FG-repeats of Nup214,
160 a NPC component known to interact with dNxf1^{UBA} (fig. S5E) (*13*). Since two copies of FG binding
161 domains (NTF2 and UBA) are minimally required for proper RNA export(*15*), dNxf2 lacks at least
162 one copy of the FG binding domain (UBA) and thus cannot export RNAs.
163
164 The predicted RNA binding domains at the N-terminus of dNxf2 imply that dNxf2 might directly
165 bind to transposon transcripts *in vivo* (Fig. 3A)(*12*). To validate this hypothesis, we performed
166 GoldCLIP/RT-qPCR experiments using an engineered OSC line in which a Halo-tag was fused to
167 the C-terminus of dNxf2 (dNxf2-Halo) (fig. S6A-F)(*16*). GoldCLIP took advantage of the covalent
168 attachment of the Halo-tag to its ligand, affording a denaturing purification of crosslinked protein-
169 RNA complexes(*17*). Strikingly, following UV crosslinking, transposon transcripts (mdg1), but not
170 rp49, remained attached to the dNxf2-Halo fusion protein despite denaturing washes (fig. S6B-C).
171 The association appeared to be direct as it depends on UV crosslinking (fig. S6B-C). Interestingly,
172 the interaction was only observed when both histone H1 and Heterochromatin Protein 1a (HP1a)
173 were depleted by RNAi, but not in the control knockdown (fig. S6B-C). This correlates with the idea
174 that the majority of transposon transcripts remain suppressed in a wildtype background and
175 therefore are not available for dNxf2 binding. Nevertheless, if the downstream silencing factors (H1
176 and HP1a) were removed, transposon transcripts could accumulate and bind dNxf2 (fig. S6B). In
177 contrast, we failed to detect any CLIP signal on Frogger despite of dramatic up-regulation of its

178 transcripts upon RNAi (fig. S6D). Since Frogger does not appear to be targeted by Piwi-piRNAs in
179 OSCs(*18*), this result suggests that the binding of dNxf2 to transposon is potentially piRNA-guided.
180 In order to obtain enough material, we performed GoldCLIP-seq experiments using dNxf2-Halo
181 knock-in OSCs depleted of Maelstrom, a piRNA pathway effector component either parallel or
182 downstream of H3K9me3 establishment on transposons(*19*). Consistent with the RT-qPCR results,
183 CLIP-seq demonstrated that dNxf2 binds to Piwi-targeted transposons (Fig. 4A). Collectively, our
184 data strongly argues that Panx and dNxf2/dNxt1 function together as a stable complex to directly
185 suppress transposons that are targeted by Piwi-piRNAs.
186
187 Loss of Panx leads to significantly decreased H3K9me3 marks over transposons(*6*, *7*). We
188 next tested if loss of dNxf2 could result in similar phenomena. Since Panx is unstable in the absence
189 of dNxf2 (fig. S2), we performed H3K9me3 ChIP-qPCR assays over several transposons while
190 driving Panx overexpression under a strong promoter (Ubiquitin). H3K9me3 changes seemed
191 rather modest upon removal of dNxf2 (fig. S8B). This result prompted us to look for alternative
192 explanations for dNxf2-mediated silencing. In this regard, dNxf1 was found to be required for
193 transposon silencing in a genome-wide RNAi screen(*10*). Additionally, female flies with mutant
194 alleles of dNxf1 are sterile and have defects in meiotic spindles(*20*), a phenotype reminiscent of
195 core piRNA pathway mutants(*21*, *22*). Hence, we tested if dNxf1 is required for Panx-mediated
196 silencing. Consistent with the RNAi screen data, germline specific depletion of dNxf1 significantly
197 impaired the repression induced by λN-Panx, thereby genetically placing dNxf1 in the Panx-
198 mediated silencing pathway (Fig. 4B). Human Nxf1/TAP has been reported to oligomerize with
199 other NXF family members to regulate RNA export(*23*, *24*). Next we tested whether dNxf2 might
200 interact with dNxf1 directly. Indeed, GFP-tagged dNxf2 can co-immunoprecipitate Halo-tagged
201 dNxf1 from OSC lysates (Fig. 4C). Further domain truncations showed that either NTF2 or UBA
202 domain of dNxf1 is sufficient to interact with the NTF2 domain of dNxf2 (Fig. 4D and fig. S10).

203 Moreover, GST pull-down assays demonstrated a direct association between dNxf1 and dNxf2 (Fig.
204 4E and fig. S11). To rule out any indirect or off-target effect of dNxf1 knockdowns, we re-introduced
205 either wild-type dNxf1 or a truncated dNxf1 missing the RNA binding domains (ΔRBD=RRM+LRR)
206 driven by Ubiquitin promoter. As expected, wild-type dNxf1 suppressed the transposon
207 overexpression caused by the shRNA targeting the 5' untranslated region of endogenous dNxf1
208 (Fig. 4F). Importantly, the truncated dNxf1 lacking the RNA cargo binding domains (ΔRBD)
209 maintained the ability to rescue transposon silencing (Fig. 4F). Because the RBD of dNxf1 is
210 required for RNA export, our results strongly argue against an indirect involvement of dNxf1 in
211 transposon suppression. Next, we sort to directly visualize potential changes in RNA localization
212 by using a rapamycin-induced tethering system (Fig. 4G and fig. S7). GFP mRNAs containing 10
213 copies of BoxB binding sites tethered with λN-FKBP are mostly localized in the cytoplasm (Fig. 4G).
214 Upon Rapamycin treatment, λN-FKBP dimerizes with FRB-dNxf2 fusion protein, allowing tethering
215 of dNxf2 to the GFP mRNAs. Intriguingly, GFP mRNAs tethered with FRB-dNxf2 start to
216 accumulate at nuclear peripheries (Fig. 4G). The effect is specific to dNxf2 because FRB alone
217 failed to cause any change. Given these properties, we named this multi-protein complex as
218 Pandas (Panx-Nxf2 dependent TAP/p15 silencing). Our data raise the possibility that deterring
219 dNxf1's function in transposon RNA export may be a key event in the process of piRNA-guided
220 silencing (fig. S12).
221
222 Like any coding mRNA, if not restrained by Piwi-piRNAs, transposon transcripts would likewise
223 be transported into the cytoplasm by the dNxf1/dNxt1 exporting machinery(*13*). In piRNA-guided
224 TGS, dNxf2/dNxt1 may function together with Panx as a stable complex to counteract this process
225 (fig. S12). As shown by our structural analysis, dNxf2^{UBA} has evolved to lose its ability to bind the
226 NPC (fig. S5). Accordingly, part of dNxf2's silencing function may be hijacking the RNA exporting
227 machinery and repurposing dNxf1 into a "dead-end" complex, hence trapping transposon

228 transcripts within the nucleus (Fig. 4G). In this regard, dNxf1 can localize to nuclear peripheries in
229 which most constitutive heterochromatin resides(*12*, *25*-*27*). Sequestering transposons to these
230 compartments via the Pandas complex may help to establish/maintain their heterochromatic state
231 (fig. S9)(*26*, *27*). Therefore, dNxf2 is likely to function in the Pandas complex to combat transposon
232 expression, at least in part by preventing transposon RNA export (fig. S12).

233 **REFERENCES**

234 1. D. T. Ge, P. D. Zamore, Small RNA-directed silencing: the fly finds its inner fission yeast?
235 *Curr. Biol.* **23**, R318–20 (2013).

236 2. R. Martienssen, D. Moazed, RNAi and heterochromatin assembly. *Cold Spring Harb*
237 *Perspect Biol*. **7**, a019323 (2015).

238 3. B. Czech, G. J. Hannon, One Loop to Rule Them All: The Ping-Pong Cycle and piRNA-
239 Guided Silencing. *Trends Biochem. Sci.* **0** (2016), doi:10.1016/j.tibs.2015.12.008.

240 4. D. M. Ozata, I. Gainetdinov, A. Zoch, D. X. N. O. X. Carroll, P. D. Zamore, PIWI-interacting
241 RNAs: small RNAs with big functions. *Nat. Rev. Genet.*, 1–20 (2018).

242 5. I. Gainetdinov, C. Colpan, A. Arif, K. Cecchini, P. D. Zamore, A Single Mechanism of
243 Biogenesis, Initiated and Directed by PIWI Proteins, Explains piRNA Production in Most
244 Animals. *Mol. Cell*. **71**, 775–790.e5 (2018).

245 6. Y. Yu *et al.*, Panoramix enforces piRNA-dependent cotranscriptional silencing. *Science*.
246 **350**, 339–342 (2015).

247 7. G. Sienski *et al.*, Silencio/CG9754 connects the Piwi-piRNA complex to the cellular
248 heterochromatin machinery. *Genes Dev.* **29**, 2258–2271 (2015).

249 8. B. Czech, J. B. Preall, J. McGinn, G. J. Hannon, A transcriptome-wide RNAi screen in the
250 Drosophila ovary reveals factors of the germline piRNA pathway. *Mol. Cell*. **50**, 749–761
251 (2013).

252 9. F. Muerdter *et al.*, A genome-wide RNAi screen draws a genetic framework for transposon
253 control and primary piRNA biogenesis in Drosophila. *Mol. Cell*. **50**, 736–748 (2013).

254 10. D. Handler *et al.*, The genetic makeup of the Drosophila piRNA pathway. *Mol. Cell*. **50**,
255 762–777 (2013).

256 11. K. G. Guruharsha *et al.*, A protein complex network of Drosophila melanogaster. *Cell*. **147**,
257 690–703 (2011).

258 12. A. Herold, T. Klymenko, E. Izaurralde, NXF1/p15 heterodimers are essential for mRNA
259 nuclear export in Drosophila. *RNA*. **7**, 1768–1780 (2001).

260 13. J. Katahira, Nuclear export of messenger RNA. *Genes (Basel)*. **6**, 163–184 (2015).

261 14. F. Port, H.-M. Chen, T. Lee, S. L. Bullock, Optimized CRISPR/Cas tools for efficient
262 germline and somatic genome engineering in Drosophila. *Proc. Natl. Acad. Sci. U.S.A.* **111**,
263 E2967–76 (2014).

264 15. I. C. Braun, A. Herold, M. Rode, E. Izaurralde, Nuclear export of mRNA by TAP/NXF1
265 requires two nucleoporin-binding sites but not p15. *Mol. Cell. Biol.* **22**, 5405–5418 (2002).

266 16. D. Savic *et al.*, CETCh-seq: CRISPR epitope tagging ChIP-seq of DNA-binding proteins.
267 *Genome Res.* **25**, 1581–1589 (2015).

268 17. J. Gu *et al.*, GoldCLIP: Gel-omitted Ligation-dependent CLIP. *Genomics Proteomics*
269 *Bioinformatics*. **16**, 136–143 (2018).

270 18. Y. W. Iwasaki *et al.*, Piwi Modulates Chromatin Accessibility by Regulating Multiple Factors
271 Including Histone H1 to Repress Transposons. *Mol. Cell*. **63**, 408–419 (2016).

272 19. G. Sienski, D. Dönertas, J. Brennecke, Transcriptional silencing of transposons by Piwi and
273 maelstrom and its impact on chromatin state and gene expression. *Cell*. **151**, 964–980
274 (2012).

275 20. E. V. Golubkova *et al.*, Dm nxf1/sbr gene affects the formation of meiotic spindle in female
276 Drosophila melanogaster. *Chromosome Res.* **17**, 833–845 (2009).

277 21. B. Czech, G. J. Hannon, A Happy 3' Ending to the piRNA Maturation Story. *Cell*. **164**, 838–
278 840 (2016).

279 22. J. S. Khurana, W. Theurkauf, piRNAs, transposon silencing, and Drosophila germline
280 development. *J. Cell Biol.* **191**, 905–913 (2010).

281 23. L. H. Matzat, S. Berberoglu, L. Lévesque, Formation of a Tap/NXF1 homotypic complex is
282 mediated through the amino-terminal domain of Tap and enhances interaction with
283 nucleoporins. *Mol. Biol. Cell*. **19**, 327–338 (2008).

284 24. S. Aibara, J. Katahira, E. Valkov, M. Stewart, The principal mRNA nuclear export factor
285 NXF1:NXT1 forms a symmetric binding platform that facilitates export of retroviral CTE-
286 RNA. *Nucleic Acids Res.* **43**, 1883–1893 (2015).

287 25. D. E. Kerkow *et al.*, The structure of the NXF2/NXT1 heterodimeric complex reveals the
288 combined specificity and versatility of the NTF2-like fold. *J. Mol. Biol.* **415**, 649–665 (2012).

289 26. B. van Steensel, A. S. Belmont, Lamina-Associated Domains: Links with Chromosome
290 Architecture, Heterochromatin, and Gene Repression. *Cell*. **169**, 780–791 (2017).

291 27. B. D. Towbin, P. Meister, S. M. Gasser, The nuclear envelope--a scaffold for silencing?
292 *Curr. Opin. Genet. Dev.* **19**, 180–186 (2009).

293 28. K. Saito *et al.*, A regulatory circuit for piwi by the large Maf gene traffic jam in Drosophila.
294 *Nature*. **461**, 1296–1299 (2009).

295 29. C. D. Armour *et al.*, Digital transcriptome profiling using selective hexamer priming for
296 cDNA synthesis. *Nat. Methods*. **6**, 647–649 (2009).

297 30. M. Martin, Cutadapt removes adapter sequences from high-throughput sequencing reads.
298 *EMBnet.journal*. **17**, 10–12 (2011).

299 31. A. Dobin *et al.*, STAR: ultrafast universal RNA-seq aligner. *Bioinformatics*. **29**, 15–21
300 (2013).

301 32. M. E. Ritchie *et al.*, limma powers differential expression analyses for RNA-sequencing and
302 microarray studies. *Nucleic Acids Res.* **43**, e47–e47 (2015).

303 33. E. Radion *et al.*, Key role of piRNAs in telomeric chromatin maintenance and telomere

304 nuclear positioning in Drosophila germline. *Epigenetics Chromatin*. **11**, 40 (2018).

305 34. P. D. Adams *et al.*, PHENIX: a comprehensive Python-based system for macromolecular
306 structure solution. *Acta Crystallogr. D Biol. Crystallogr.* **66**, 213–221 (2010).

307 35. P. Emsley, K. Cowtan, Coot: model-building tools for molecular graphics. *Acta Crystallogr.*
308 *D Biol. Crystallogr.* **60**, 2126–2132 (2004).

309 36. A. Waterhouse *et al.*, SWISS-MODEL: homology modelling of protein structures and
310 complexes. *Nucleic Acids Res.* **46**, W296–W303 (2018).

311 37. H. McWilliam *et al.*, Analysis Tool Web Services from the EMBL-EBI. *Nucleic Acids Res.*
312 **41**, W597–600 (2013).

313 38. X. Robert, P. Gouet, Deciphering key features in protein structures with the new ENDscript
314 server. *Nucleic Acids Res.* **42**, W320–4 (2014).

315

316

317 **Figure 1. dNxf2 functions as a cofactor of Panx in the piRNA pathway.**

318 **A**, Western blots showing co-immunoprecipitation of endogenous dNxf2 with GFP-Panx from ovary
319 lysates. Two different rabbit polyclonal monospecific dNxf2 (dNxf2-N and dNxf2-C) antibodies were
320 used to detect endogenous dNxf2. **B**, Halo-ligand staining and western blots showing co-
321 immunoprecipitation of endogenous Panx with dNxf2-Halo driven by the endogenous dNxf2
322 promoter from OSC lysates. A rabbit polyclonal monospecific Panx antibody was used to detect
323 endogenous Panx. Left panel shows depletion of dNxf2-Halo proteins in the unbound sample by
324 Halo beads, and the anti-Tubulin blots serve as loading controls; Right panel shows endogenous
325 Panx proteins. **C**, The effects of germline (*nanos*-GAL4) knockdown of the indicated genes on
326 Renilla-normalized Firefly luciferase activity of the reporter while tethering λN-Panx. For
327 comparison, the relative value of the attp2 control was used for normalization. Data show
328 mean ± s.d. (n = 15; *P = 1.41387E-07). **D**, Comparison of steady-state RNA levels are shown as
329 reads per million (rpm) mapping to the sense strand of each transposon consensus from the *nanos*-
330 GAL4 driven knockdown for dNxf2 (Y axis) versus control (X axis). Dashed lines indicate two-fold
331 changes. The average of two replicates is shown. KD = knockdown. Red dots indicate transposon
332 elements with significant changes. **E**, Comparison of steady-state RNA levels (RNA-seq; shown
333 as RPM) mapping to the sense strands of each transposon consensus from the *nanos*-GAL4 driven
334 knockdowns of the indicated genes. Red dots indicate transposon elements with significant
335 changes from **D**. **F**, Heat map displaying steady-state RNA levels (RNA-seq) as reads per million
336 (rpm) for top 70 detected transposons from the *nanos*-GAL4 driven knockdowns of the indicated
337 genes in a blue-white scale.

338

339 **Figure 2. The UBA domain of dNxf2 interacts with Panx directly.**

340 **A**, Domain architectures of Panx, dNxf2, dNxf1, and dNxt1 are shown. Numbers above the
341 diagrams correspond to amino acid residues of each protein. Domain names are abbreviated within
342 respective colored region. **B-E**, Y2H assays mapping the interacting regions between *Drosophila*
343 Nxf1/2 and Panx or dNxt1. Interactions were determined by either measuring the beta-
344 galactosidase activity produced by the reporter gene or growth on YSD media lacking the indicated
345 essential amino acid or Uracil. Data are averages of three independent experiments (n=3). Proteins
346 or fragments shown above the dashed line are used as preys in the assays. **B**, Y2H assays
347 mapping regions of *Drosophila* Nxf1/2 that interact with Panx. **C**, Y2H assays mapping regions of
348 *Drosophila* Nxf1/2 that interact with dNxt. **D**, Yeast three hybrid determining the requirement of
349 dNxt1 for Nxf2:Panx interaction. **E**, Y2H assays mapping minimum regions of Panx that interact
350 with $dNxf2^{UBA}$. **F**, Left panel shows the size exclusive chromatography profile of the NTF2 and UBA
351 domains of dNxf2 forming heterodimers with dNxt1 and $Panx^{NIR}$ in solution, respectively. A dNxf2
352 fragment spanning the NTF2 and UBA domains that is covalently linked to $Panx^{NIR}$ forms a stable
353 complex with dNxt1. Right panel, SDS-PAGE shows the components of the peak in the elution
354 profile. Color schemes used for the three complexes are indicated in the key. **G**, Quantification of
355 the dissociation constant for the interaction between $dNxf2^{UBA}$ and $Panx^{NIR}$ as measured by an
356 isothermal titration calorimetry assay.

357

358

359

360

361

362

363

364 **Figure 3. Structure of dNxf2^{UBA} in complex with Panx^{NIR}.**

365 **A**, Schematic of interacting region between dNxf2 and Panx. Numbers above or below the
366 diagrams correspond to amino acid residues of dNxf2 or Panx, respectively. Domain names are
367 abbreviated within respective colored region. NIR, dNxf2 interacting region. **B**, Left, cartoon
368 representation of dNxf2^{UBA} in complex with Panx^{NIR}. The dNxf2^{UBA} and Panx^{NIR} fragment are
369 colored in wheat and teal, respectively. Right, a view rotated 90° around the vertical axis. **C**,
370 Electrostatic potential analysis showing the Panx-binding surface of dNxf2^{UBA}. Panx^{NIR} is shown in
371 cartoon mode. **D**, A detailed view showing the interactions between dNxf2^{UBA} and Panx^{NIR}. Key
372 residues involved in binding are shown in sticks. Close-up views of hydrophobic interactions
373 between dNxf2^{UBA} and Panx^{NIR} are shown on the right. **E**, Y2H assays measuring the binding of
374 wild-type or mutant dNxf2^{UBA} with Panx^{NIR}. Mutations of key residues are indicated along the bars.
375 **F**, Western blots and Halo-ligand staining showing co-immunoprecipitation of GFP-tagged Panx or
376 its NIR deletion mutant (ΔNIR) with Halo-tagged dNxf2 or its F826A/I827A double mutant from OSC
377 cells. GFP serves as a negative control. **G**, Effects of the indicated λN fusion proteins or a non-
378 tethering control (GFP-dNxf2) on luciferase activity of the reporters integrated into the attP2 landing
379 site. Data show mean ± s.d. (n = 15; *P = 1.41387E-07). **H**, The effects of λN-dNxf2 tethering on
380 luciferase activity of reporters with increasing number of BoxB sites. All reporters are integrated
381 into the same genomic locus (attP2 landing site). Fold repression is calculated as total protein-
382 normalized Firefly luciferase luminescent values of the control (no tethering) divided by that of the
383 indicated experiments. Data show mean ± s.d. (n = 15; *P = 1.41387E-07).

384

385

386 **Figure 4. The Pandas complex is required for piRNA-guided transposon silencing.**

387 **A**, Comparison of GoldCLIP-seq are shown as reads per million (rpm) mapping to the sense strand
388 of each transposon consensus for Maelstrom (*X* axis) versus a LacZ control knockdown (*Y* axis).
389 A mammalian spike-in was used to normalize different samples. Dashed lines indicate two-fold
390 changes. The pooled reads from two replicates are shown. Red dots indicate Piwi-targeted
391 transposons, blue dots indicate H1-dependent transposons and green dots indicate other
392 transposons. B, The effects of germline specific knockdown (nanos-GAL4) of the indicated genes
393 on Renilla-normalized Firefly luciferase activity of the reporter while tethering λN-Panx. For
394 comparison, the results from Fig. 1C (Egg, attp2 and Zuc) were shown here again. Data show
395 mean ± s.d. (n = 15; *P = 1.41387E-07). **C**, Western blots and Halo-ligand staining showing co-
396 immunoprecipitation of GFP-tagged dNxf2 with Halo-tagged dNxf1 from OSC cells. ΔNTF2, Halo-
397 dNxf1 lacking the NTF2 domain, and GFP serves as a negative control. **D**, Western blots and Halo-
398 ligand staining showing co-immunoprecipitation of Halo-tagged dNxf2-NTF2 domain with different
399 domain truncations of GFP-tagged dNxf1 from OSC cells. ΔRBD, dNxf1 lacking the N-terminus
400 RRM and LRR domains; GFP serves as a negative control. **E**, SDS-PAGE showing pulldown
401 results of the Nxf2$^{NTF2+UBA}$-(GS)4-Panx^{NIR}/dNxt1 complex by either GST-tagged dNxf1-NTF2 or
402 dNxf1-(NTF2+UBA) respectively, compared to a GST control. **F**, RT-qPCR results showing the
403 effects of germline (*nanos*-GAL4) knockdown of the indicated genes in the presence or absence of
404 different transgenes. Fold changes are calculated as rp49-normalized RNA levels divided by that
405 of the corresponding controls. Mean values ± s.d. from 3 independent experiments are shown. **G**,
406 SIM super-resolution microscopy of RNA FISH detected by HCR2.0. Data showing the comparison
407 of the localizations of the reporter mRNAs tethered with λN-FKBP, upon transient recruitment of
408 either FRB-dNxf2 or FRB alone when treated with rapamycin for 2 hours to induce FKBP:FRB
409 dimerization. Top panel, RNA signal (red) with DAPI staining; middle, DAPI staining (blue); bottom,
410 RanGAP-GFP fusion protein (green) were shown. The scale bar represent 5 μM in length.

Figure 1

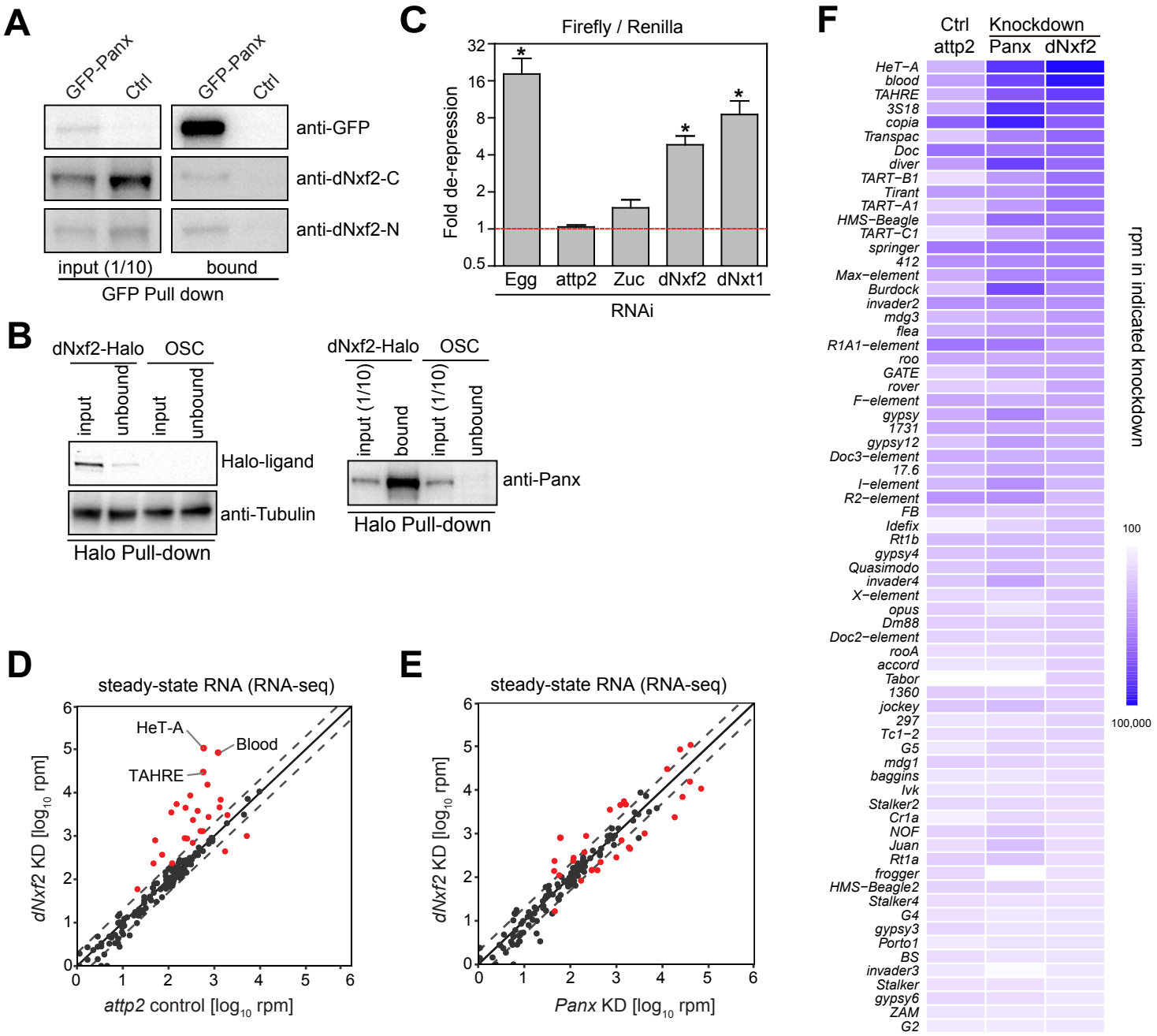
A
GFP-Panx
Ctrl
GFP-Panx
Ctrl
anti-GFP
anti-dNxf2-C
anti-dNxf2-N
input (1/10)
bound
GFP Pull down
B
dNxf2-Halo
OSC
input
unbound
input
unbound
Halo-ligand
anti-Tubulin
Halo Pull-down
dNxf2-Halo
OSC
input (1/10)
bound
input (1/10)
unbound
anti-Panx
Halo Pull-down
C
Firefly / Renilla
Fold de-repression
32
16
8
4
2
1
0.5
Egg
attp2
Zuc
dNxf2
dNxt1
RNAi
D
steady-state RNA (RNA-seq)
HeT-A
Blood
TAHRE
dNxf2 KD [log10 rpm]
attp2 control [log10 rpm]
E
steady-state RNA (RNA-seq)
dNxf2 KD [log10 rpm]
Panx KD [log10 rpm]
F
Ctrl
Knockdown
attp2
Panx
dNxf2
HeT-A
blood
TAHRE
3S18
copia
Transpac
Doc
diver
TART-B1
Tirant
TART-A1
HMS-Beagle
TART-C1
springer
412
Max-element
Burdock
invader2
mdg3
flea
R1A1-element
roo
GATE
rover
F-element
gypsy
1731
gypsy12
Doc3-element
17.6
I-element
R2-element
FB
Idefix
Rt1b
gypsy4
Quasimodo
invader4
X-element
opus
Dm88
Doc2-element
rooA
accord
Tabor
1360
jockey
297
Tc1-2
G5
mdg1
baggins
Ivk
Stalker2
Cr1a
NOF
Juan
Rt1a
frogger
HMS-Beagle2
Stalker4
G4
gypsy3
Porto1
BS
invader3
Stalker
gypsy6
ZAM
G2
rpm in indicated knockdown
100
100,000

Figure 2

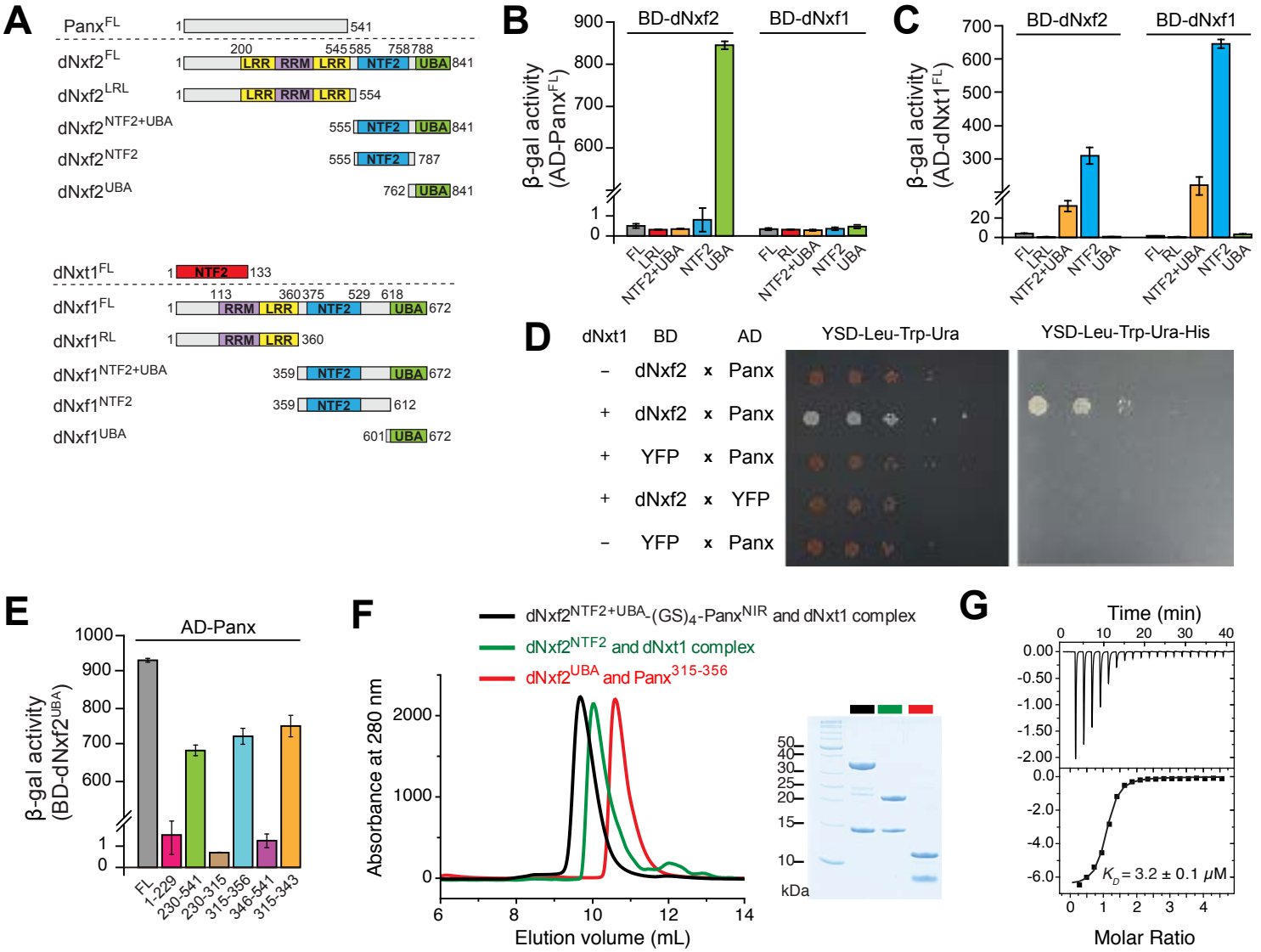
A
Panx^FL
dNxf2^FL
dNxf2^LRL
dNxf2^NTF2+UBA
dNxf2^NTF2
dNxf2^UBA
LRR
RRM
NTF2
UBA
dNxt1^FL
dNxf1^FL
dNxf1^RL
dNxf1^NTF2+UBA
dNxf1^NTF2
dNxf1^UBA
B
BD-dNxf2
BD-dNxf1
β-gal activity (AD-Panx^FL)
FL
LRL
NTF2+UBA
NTF2
UBA
RL
C
β-gal activity (AD-dNxt1^FL)
D
dNxt1
BD
AD
YSD-Leu-Trp-Ura
YSD-Leu-Trp-Ura-His
dNxf2 x Panx
YFP x Panx
dNxf2 x YFP
E
AD-Panx
β-gal activity (BD-dNxf2^UBA)
FL
1-229
230-541
230-315
315-356
346-541
315-343
F
dNxf2^NTF2+UBA-(GS)4-Panx^NIR and dNxt1 complex
dNxf2^NTF2 and dNxt1 complex
dNxf2^UBA and Panx^315-356
Absorbance at 280 nm
Elution volume (mL)
kDa
G
Time (min)
K_D = 3.2 ± 0.1 μM
Molar Ratio

Figure 3

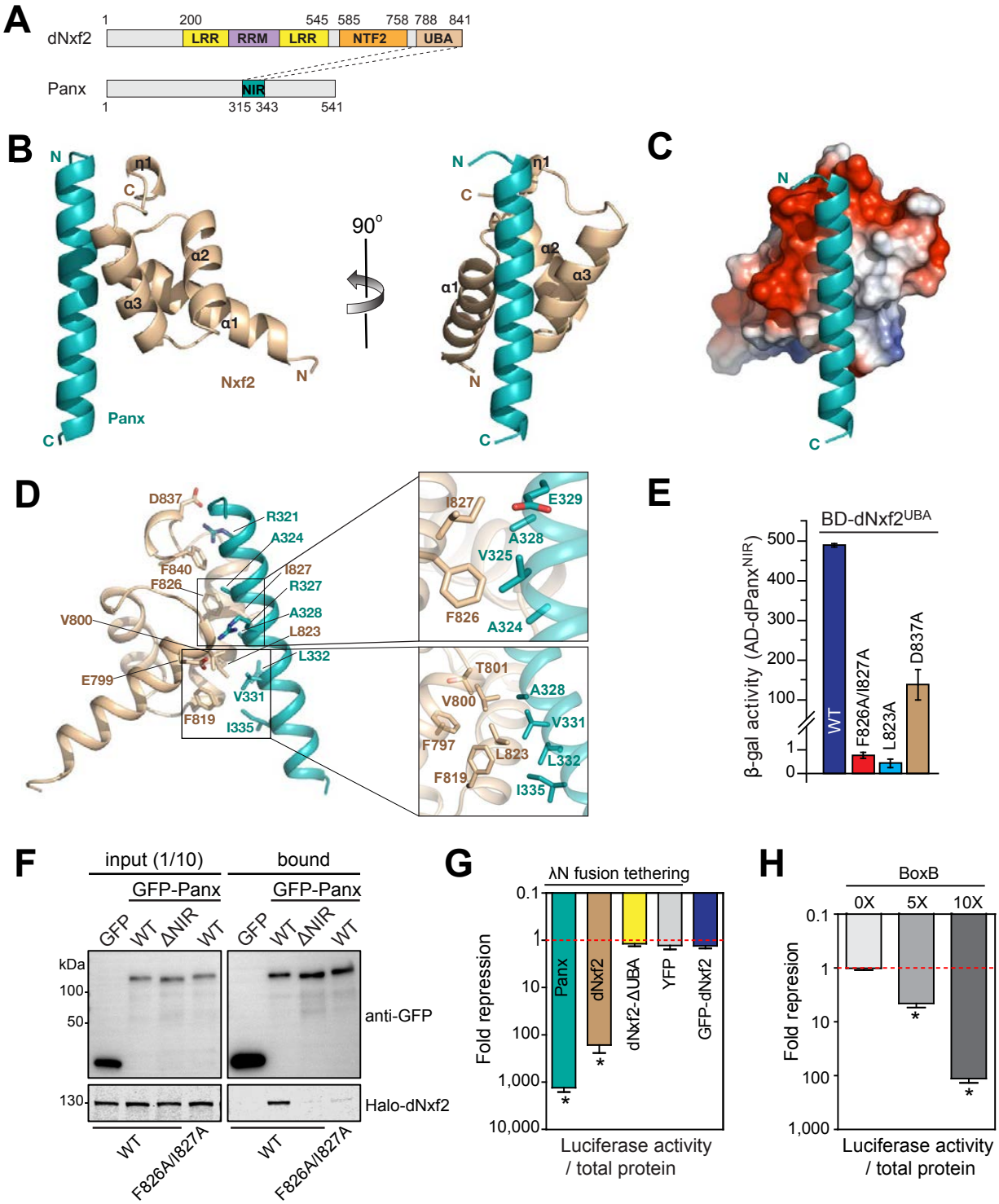
A
dNxf2
1
200
545
585
758
788
841
LRR
RRM
LRR
NTF2
UBA
Panx
NIR
1
315 343
541
B
N
η1
C
α2
α3
α1
Nxf2
N
Panx
C
90°
N
η1
C
α2
α3
α1
N
C
C
N
C
D
D837
R321
A324
F840
F826
I827
R327
V800
A328
L823
L332
E799
V331
F819
I335
I827
E329
A328
V325
F826
A324
T801
V800
A328
V331
F797
L823
L332
F819
I335
E
BD-dNxf2UBA
β-gal activity (AD-dPanxNIR)
500
400
300
200
100
1
0
WT
F826A/I827A
L823A
D837A
F
input (1/10)
bound
GFP-Panx
GFP-Panx
GFP
WT
ΔNIR
WT
GFP
WT
ΔNIR
WT
kDa
100
50
anti-GFP
130
Halo-dNxf2
WT
F826A/I827A
WT
F826A/I827A
G
λN fusion tethering
Fold repression
0.1
1
10
100
1,000
10,000
Panx
dNxf2
dNxf2-ΔUBA
YFP
GFP-dNxf2
Luciferase activity
/ total protein
H
BoxB
0X
5X
10X
Fold repression
0.1
1
10
100
1,000
Luciferase activity
/ total protein

Figure 4

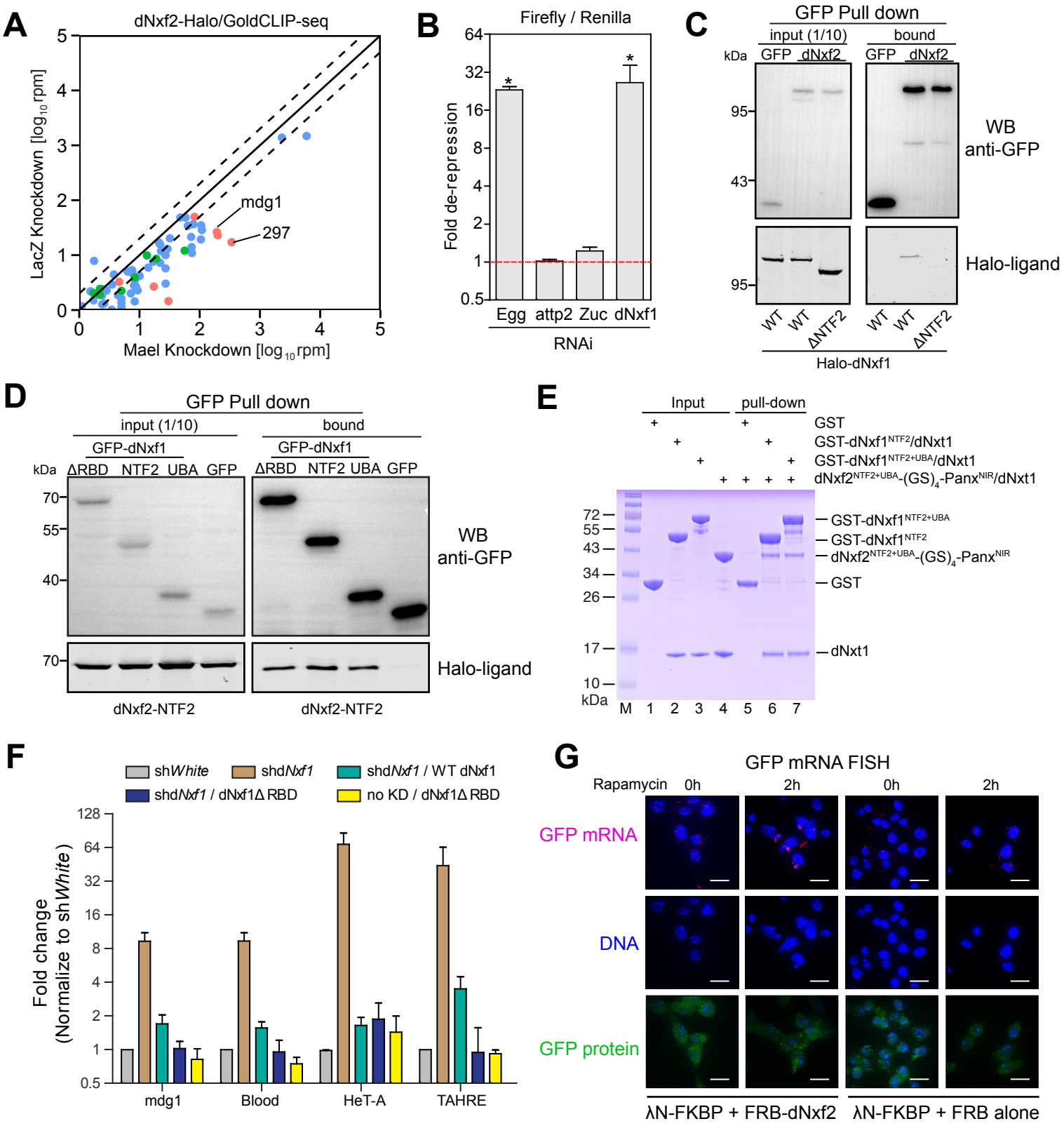
A
dNxf2-Halo/GoldCLIP-seq
LacZ Knockdown [log10 rpm]
Mael Knockdown [log10 rpm]
mdg1
297
B
Firefly / Renilla
Fold de-repression
Egg
attp2
Zuc
dNxf1
RNAi
C
GFP Pull down
input (1/10)
bound
kDa
GFP
dNxf2
WB anti-GFP
Halo-ligand
WT
ΔNTF2
Halo-dNxf1
D
GFP Pull down
input (1/10)
bound
GFP-dNxf1
ΔRBD
NTF2
UBA
GFP
WB anti-GFP
Halo-ligand
dNxf2-NTF2
E
Input
pull-down
GST
GST-dNxf1NTF2/dNxt1
GST-dNxf1NTF2+UBA/dNxt1
dNxf2NTF2+UBA-(GS)4-PanxNIR/dNxt1
GST-dNxf1NTF2+UBA
GST-dNxf1NTF2
dNxf2NTF2+UBA-(GS)4-PanxNIR
GST
dNxt1
kDa
M
F
shWhite
shdNxf1
shdNxf1 / WT dNxf1
shdNxf1 / dNxf1ΔRBD
no KD / dNxf1ΔRBD
Fold change (Normalize to shWhite)
mdg1
Blood
HeT-A
TAHRE
G
GFP mRNA FISH
Rapamycin
0h
2h
GFP mRNA
DNA
GFP protein
λN-FKBP + FRB-dNxf2
λN-FKBP + FRB alone